Dynamic Analysis and Speed Control of a Novel Micro-platform Driven by Vibrating Motors

Panagiotis Vartholomeos and Evangelos Papadopoulos
Department of Mechanical Engineering, National Technical University of Athens
15780 Athens, Greece
{barthol, egpapado}@central.ntua.gr

ABSTRACT
This paper presents the dynamic analysis and speed control of a novel micro-robotic platform that is able to move with sub-micrometer positioning accuracy at velocities up to 1.5 *mm/s*. The platform actuation system employs vibration micro-motors. The motion principle is discussed. The dynamic model of the platform and of its actuation system is developed and its operating constraints are analytically expressed. Emphasis is given on the periodic orbits that the platform may exhibit under specific driving conditions. Closed-loop speed control of the vibrating actuators is implemented. The micro-robot design is simple, compact, of low cost and allows for untethered power supply using simple means such as single cell batteries.

KEY WORDS
micro-robot, micro-positioning, vibration motors, feedback control.

1. Introduction
In the last decade, micro-robotics has become an increasingly important field of research. Domains of application such as micro fabrication, biotechnology, microscopy and opto-electronics, demand miniaturized or micro-robotic platforms that provide ultra high precision, flexibility and a wide mobility range. To this aim, extensive research has been carried out in the design and realization of micro-manipulators and of micro-robots. Motion principles and actuation mechanisms that combine sub-micrometer motion of high resolution and the speed virtues of coarse positioning have been the subject of intensive studies.
Several micro-actuation techniques have been devised and are usually based on smart materials such as piezo-electric actuators, shape memory alloys, etc. The most popular micro-positioning motion mechanism is the stick-slip principle, which is implemented using piezoelectric actuators. This principle is employed by the 3DOF micro-robotic platform presented in [1], by the MINIMAN micro-robot presented in [2-3] and by the MiCRoN robot presented in [4]. These platforms are capable of positioning accuracy of less than 200*nm* and provide velocities of up to a few *mm/s*. The impact drive principle is employed by the 3DOF micro-robotic platform Avalon which provides step size of about 3.0 *μm* and speeds up to 1 *mm/s*, and is presented in [5-6]. A different motion mechanism based on piezo-tubes is utilized by the Nano Walker micro-robot presented in [7].
Although piezoelectric actuators seem to be the favored smart material for micro-positioning and do provide the required positioning resolution and actuation response, they usually suffer from complex power units that are expensive and cumbersome and which do not easily allow for untethered operation. Furthermore, piezoelectric actuators are complex systems that exhibit non-linear behavior and as a result they lack an accurate mathematical model that can provide a reliable prediction of the system's behavior.
This paper presents a novel, simple and compact micro-robotic platform [8] that is able to perform translational and rotational sliding with sub-micrometer positioning accuracy and velocities up to 1.5*mm/s*. All the components of the mechanism including its driving units are of low cost and readily available. The motion mechanism is based on the interaction of centripetal forces due to vibrating micro-motors and friction forces at the base supports. The concept was inspired by observing the motion of devices that vibrate, such as cellular phones or unbalanced washing machines, [9, 10]. First, analysis of the motion principle physics is provided. Then, rigid and deformable body dynamic models of the platform are developed. Also the dynamics of the actuators are presented. The modes of operation of the platform are defined, and simulation is performed to demonstrate periodic orbits that the platform may exhibit under specific operating conditions. Finally, closed loop speed control using feedback linearization is implemented to control and improve the speed response of the platform and to compensate for modeling errors.

2. Motion Principle
The motion principle is first demonstrated using a simplified single degree-of-freedom (DOF) mobile platform of mass *M*. The motion mechanism employs an eccentric mass *m* rotated by a motor *O* mounted on the platform as shown in Fig. 1.

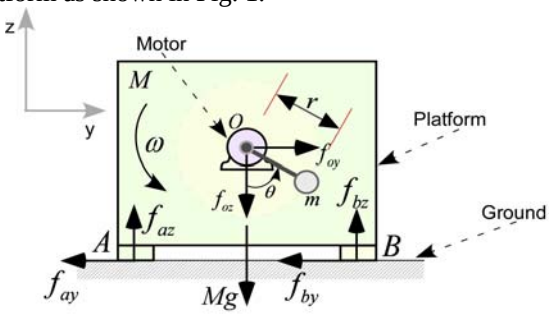

Fig. 1 Simplified 1DOF platform with rotating mass *m*.

It is assumed that the mass *m* rotates on a vertical plane at constant angular speed ω, about point *O* and that the platform is constrained to move along the y-axis only. One cycle of operation is completed when the mass has described an angle of 360^o. Gravitational and centripetal forces exerted on the rotating mass are resolved along the y-z axis to yield:

$$f_{oy} = mr\omega^2 \sin\theta$$
$$f_{oz} = -mg - mr\omega^2 \cos\theta \quad (1)$$

where g is the acceleration of gravity and r the length of the link between *m* and *O*. These forces are also applied to the platform at point *O*, while the moment due to the small eccentric mass is neglected. When the angular speed ω is low, the platform does not move because the horizontal actuation force f_{oy} is cancelled by frictional forces at the platform support points A and B. However, if the angular speed ω exceeds a critical value, then f_{oy} overcomes the Coulomb friction forces applied at the two support points, and as a result, the platform begins to slide.

Using a simplified static-kinetic friction model, [11], the equations of motion along the y and z axes during motion of the platform are given by the following equations:

$$M\ddot{y} = f_{oy} - f_{fr}$$
$$0 = f_{az} + f_{bz} + (-Mg + f_{oz}) \quad (2)$$
$$f_{fr} = f_C(f_{az} + f_{bz})sign(\dot{y})$$

where all forces are defined in Fig. 1, *M* is the mass of the platform, f_{fr} is friction and f_C is the Coulomb level.

The platform response is obtained by means of a numerical simulation of eqs. (2) and the results are displayed in Fig. 2.

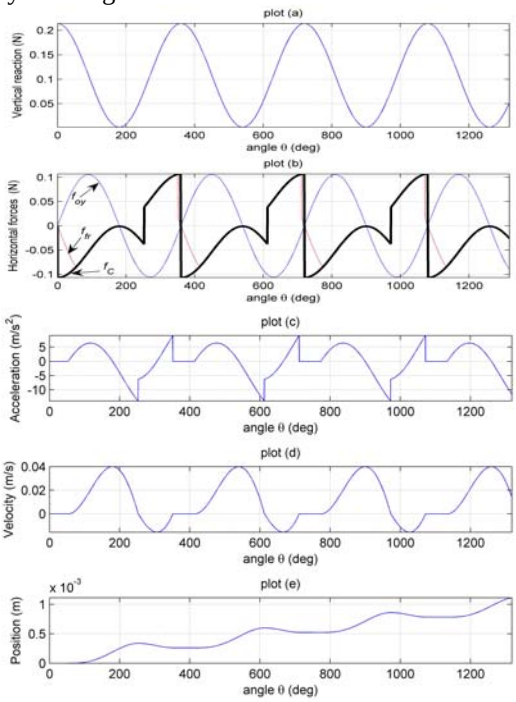

Fig. 2. Forces applied to 1DOF platform and resulting motion variables

Fig. 2a depicts the time response of the sum of the vertical forces exerted on the platform, i.e. the actuation force component f_{oz} plus the gravitational force Mg. This sum is equal in magnitude to the support reaction forces and is time-periodic since it includes a sinusoidal and a DC component. The same applies to the Coulomb friction level, f_C, which is shown in Fig. 2b. This figure also shows the horizontal forces that act upon the platform, namely the horizontal actuation force f_{oy} and the friction force f_{fr}. Fig. 2c depicts the acceleration of the platform $\ddot{y}$, while Fig. 2d depicts its velocity, and Fig. 2e its displacement. From Figs. 2b and 2d, it is clear that motion is induced when the horizontal actuation force overcomes the static friction limit f_C. Quite interestingly as shown in Fig. 2e, for a counterclockwise rotation of the motor, the platform exhibits a net displacement along the positive y-axis. This motion stems from the cyclic behavior of the actuation and friction forces and is explained next.

When the eccentric mass is at the lower points of its trajectory, the normal forces and therefore the frictional forces are high, whereas when the eccentric mass is at its highest points, the normal and frictional forces are low. Accordingly, for anticlockwise rotation of mass *m* initiated at $\theta = 0^o$, the platform tends not to move when *m* is at a low position and to move to the right when the mass is at high one. When *m* passes the highest point $\theta = 180^\circ$, the platform already has a non-zero velocity. As *m* moves past this point, friction forces together with actuation forces tend to decelerate the platform and even change its direction. As friction still increases eventually brings the platform to a stop. The actuation forces are now pointing to the left and as a result reverse platform motion is induced. Since the platform velocity became zero past the 180^o point, there is less time for it to accelerate in the opposite direction and finally return back to its initial position before stopping again. Therefore, once a cycle is completed, the platform exhibits a net displacement as shown in Fig. 2e. Reversal of the direction of ω will lead to a reversal of the direction of motion.

3 3DOF Platform

The motion principle presented previously is employed in this section for the design of a 3 degree-of freedom (dof) mobile mini robot. The design of the mini robot must meet the following design objectives: The platform should be capable of performing x, y, θ motion. It should be able to reach positioning resolution of the order of sub-microns. The platform should also be able to travel long distances, i.e. it should be able to scan a workspace whose area is five to ten times the dimensions of the platform. It should develop speeds of the order of several mm/s. Its size should be less than $5\,cm^2$ so that multi-robot cooperation within a workspace of limited area would be feasible. Finally the cost of constructing and powering the platform should be as small as possible. To this aim the following design was favored [8]:

The geometry of the base of the micro-robot is an equilateral triangle of length l. Three small rigid supports A, B, and C located at each vertex of the triangle provide the contact points between the platform and the ground, see Fig. 3. The actuation of the platform employs miniature-vibrating motors. Three identical vibrating motors D, E and F, are symmetrically mounted on top of the platform as shown in Fig. 3.

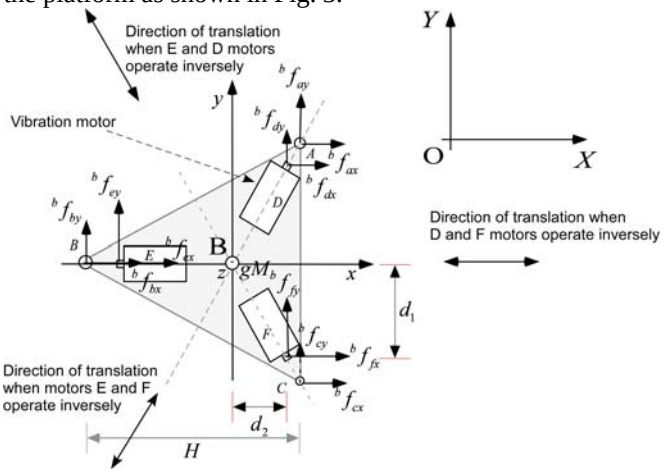

Fig. 3. Actuation and reaction forces applied on the platform

If actuators D and F spin at an opposite sense of rotation while E is inactive, then the platform slides along the positive x-axis, if their sense of rotation is reversed then sliding occurs along the negative x-axis. Similarly when motors D and E or E and F spin at the same speed and opposite sense of rotation, pure translational motion is induced at an angle of 120^o or 240^o with respect to the x-axis respectively. When D, E, and F motor spin at the same speed and at the same sense of rotation, then pure rotation about the platform CM is performed.

4 Dynamics

The description of the dynamics of the micro-robotic platform requires the use of three dynamic models:

a) Rigid body platform dynamics.
b) Deformable platform dynamics.
c) Actuator dynamics

Platform dynamics The assumptions on which the platform dynamic model is based are: (i) The imbalance load can be modeled as a point mass m, rotating at a distance r from the motor axis. (ii) All actuators are identical. (iii) Every rotating mass m rotates at a constant angular speed ω and the plane of rotation is normal to the plane of the base. (iv) All rotating masses are in phase. (v) For reasons of simplicity it is assumed that the contact points of the platform experience Coulomb friction with a constant friction coefficient μ.

The platform analysis involves the body-fixed frame B_{xy} and the inertial frame O_{XY}, see Fig. 3. The adopted notation is ${}^{i}f_{j}$ where the superscript i is the frame index and subscript j is the component x,y,z index. The b superscript denotes frame B. Frame O uses no superscript.

The position vectors of the contact points A, B, and C are denoted by ${}^{b}\mathbf{r}_a, {}^{b}\mathbf{r}_b, {}^{b}\mathbf{r}_c$ and the position vectors of the motor axis points D, E and F on which the imbalance forces are applied are denoted by ${}^{b}\mathbf{r}_d, {}^{b}\mathbf{r}_e, {}^{b}\mathbf{r}_f$. Forces ${}^{b}\mathbf{f}_a, {}^{b}\mathbf{f}_b, {}^{b}\mathbf{f}_c$ include the normal and frictional contact forces at contact points A, B, and C, respectively. The angle θ, is the eccentric load angle (motor angle) with respect to the vertical axis, see Fig. 1. Due to the rotating eccentricities, forces ${}^{b}\mathbf{f}_d, {}^{b}\mathbf{f}_e, {}^{b}\mathbf{f}_f$, are applied at points D, E, and F of the platform, and moments ${}^{b}\mathbf{n}_d, {}^{b}\mathbf{n}_e, {}^{b}\mathbf{n}_f$ are applied along its motor axes, see Fig. 3. Their body-fixed components are given by,

$$\left.\begin{aligned}
{}^{b}f_{ix} &= -mr\omega^2 \sin\phi_i \sin\theta \\
{}^{b}f_{iy} &= mr\omega^2 \cos\phi_i \sin\theta \\
{}^{b}f_{iz} &= -mg - mr\omega^2 \cos\theta \\
{}^{b}n_{ix} &= -mgr \cos\phi_i \sin\theta \\
{}^{b}n_{iy} &= -mgr \sin\phi_i \sin\theta \\
{}^{b}n_{iz} &= 0
\end{aligned}\right\} \quad i = \{d, e, f\} \qquad (3)$$

where $\omega = \dot{\theta}$ is motor angular velocity, r is the eccentricity of the imbalance mass m and $\phi_i = \{60^o, 180^o, -60^o\}$ are the angles of position vectors ${}^{b}\mathbf{r}_d, {}^{b}\mathbf{r}_e, {}^{b}\mathbf{r}_f$. Then, the Newton-Euler equations of the platform are written as, [12]:

$$M\dot{\mathbf{v}} = \mathbf{R}\sum_i {}^{b}\mathbf{f}_i, \qquad i = \{a,b,c,d,e,f\} \qquad (4a)$$

$$\begin{aligned}
&{}^{b}\mathbf{I}\,{}^{b}\dot{\boldsymbol{\omega}}_p + {}^{b}\boldsymbol{\omega}_p \times {}^{b}\mathbf{I}\,{}^{b}\boldsymbol{\omega}_p = \sum_i ({}^{b}\mathbf{r}_i \times {}^{b}\mathbf{f}_i) + \sum_i {}^{b}\mathbf{n}_j \\
&i = \{a,b,c,d,e,f\},\ j = \{d,e,f\}
\end{aligned} \qquad (4b)$$

where $\mathbf{R}$ is the rotation matrix, between frames B and O, $\boldsymbol{\omega}_p$ is the platform angular velocity, ${}^{b}\mathbf{I}$ is the platform inertia matrix, and $\mathbf{v} = [\dot{x}, \dot{y}, \dot{z}]^T$ is the platform CM position in the inertial frame.

Deformable body dynamics While the platform is static and the actuation forces gradually increase, the forces distributed to the platform legs reach the Coulomb level and motion is impending. It is required to have knowledge of the force distribution on each of the three supports A, B, and C of the triangular platform during static conditions. These six unknowns can be determined by considering small deformations along the base of the platform. For this purpose, the platform is modeled as a lumped system, consisting of three point masses connected via stiff springs, see Fig. 4. The lumped masses $M_1 = M_2 = M_3$, whose aggregate equals the mass M of the base, are located at the tips of an equilateral triangle and the springs have constants $k_1 = k_2 = k_3$. The produced deformations are adequately small so that the change in the angle of the springs is considered negligible. Forces $\mathbf{f}_{ai}, \mathbf{f}_{fi}, \mathbf{f}_{si}$ with $i = \{1,2,3\}$, are the actuation, friction and spring forces exerted at mass i.

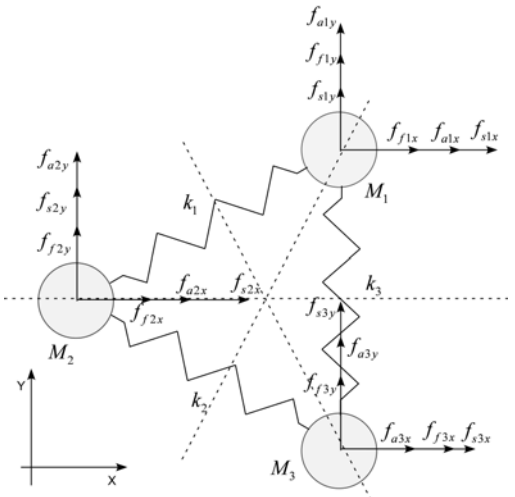

Fig. 4. Forces applied to the mass-spring model

The dynamic equations of the spring-mass system are:

$$\mathbf{M}\ddot{\mathbf{x}} = \mathbf{A}\mathbf{x} + \mathbf{f}_a + \mathbf{f}_f, \quad \mathbf{x}(0) = \mathbf{0}, \dot{\mathbf{x}}(0) = \mathbf{0} \tag{6}$$

where $\mathbf{M}$ is the mass matrix, $\mathbf{A}$ is a matrix containing spring constants, and $\mathbf{x} = [x_1, x_2, x_3, y_1, y_2, y_3]^T$ represents the x-y displacement of the three masses. When the masses are in a static state, the unknowns of the system are the six friction forces, which are determined by solving the six static equilibrium equations. In the case where some or all of the masses are in motion, then the magnitude of the corresponding friction forces is determined by the Coulomb friction limit, whereas the direction of the friction forces is determined by the velocity of the corresponding mass.

Actuator dynamics The actuator is modeled as a system comprising a DC permanent magnet motor and an imbalanced load m, see Fig. 5.

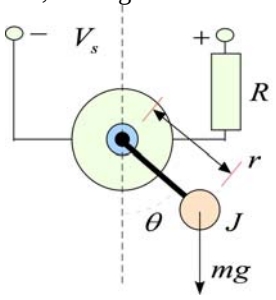

Fig. 5. Lump parameter model of the actuators

The input to the actuator is the voltage V_s. If the inductance of the windings of the motor is considered negligible, then the dynamics of the actuator are expressed through the following equation,

$$\ddot{\theta} = -\frac{k_T^2}{RJ}\dot{\theta} - \frac{mgr}{J}\sin\theta - (\frac{c}{J}sign(\dot{\theta}) + \frac{b}{J}\dot{\theta}) + \frac{k_T}{RJ}V_s \tag{7}$$

where k_T is motor's torque constant, R is its ohmic resistance, J is the inertia of the eccentric load, and the term $(\frac{c}{J}sign(\dot{\theta}) + \frac{b}{J}\dot{\theta})$ is the Coulomb and viscous friction.

5 Modes of operation

In this section, pure rotation and pure translation motion capabilities of the micro-robotic platform are examined. If at least one of the actuators is spinning, then the platform is said to be in operation. The feasible driving speeds ω define three modes of operation according to the type of motion that is induced to the platform. These are:

a) Static mode of operation
b) Closed orbit mode of operation
c) Locomotion mode of operation

Static mode of operation. As stated in Section II, if ω is below a critical value ω_{sl} i.e. $0 < \omega \le \omega_{sl}$, then the actuation forces are not large enough to induce motion. The analytical expressions of ω_{sl} for the translational and rotational cases are derived as described in [8] and are given by eqs (8) and (9) respectively.

$$\omega_{sl\,\min\,\text{trans}} = \left(\frac{\left(\frac{2\mu}{\sqrt{3}}\right) g\left(3m + M\right)}{2mr\sqrt{1 + \left(\frac{2\mu}{\sqrt{3}}\right)^2}} \right)^{1/2} \tag{8}$$

$$\omega_{sl\,\min\,\text{rot}} = \left(\frac{2g(3 + M/m)}{3r(4 + a^2\mu^{-2})^{1/2}} \right)^{1/2} \tag{9}$$

Closed orbit mode of operation. If speed ω is greater than ω_{sl}, then the actuation forces are large enough to counteract the friction forces, and consequently, to induce motion. It can be shown that for a small range of angular speeds $\omega_{sl} < \omega \le \omega_c$, the forward and reverse displacements per cycle are equal. Hence the platform performs forced oscillations about a fixed point and the net displacement over time is zero. The analytical expression of ω_c is derived by integrating the equations of motion over a cycle and by setting the forward displacement per cycle, equal to the reverse one. The translational case is given by (10).

$$\omega_c = \sqrt{\frac{\mu g(3m + M)}{3mr}} \left(3 - 4\sqrt{3}\mu\cot^{-1}(2\mu/\sqrt{3}) + (3 + 4\mu^2)\left(\cot^{-1}(2\mu/\sqrt{3})\right)^2\right)^{1/4} \tag{10}$$

For the rotational case, ω_c can be determined only numerically.

Locomotion mode of operation. For values of $\omega \ge \omega_c$, the platform begins to exhibit net displacement per cycle. If ω is very large i.e., if it exceeds the critical value ω_{tip}, then *tipping* occurs and platform stability is lost. The range of the driving speeds $\omega \in [\omega_c, \omega_{tip}]$ is defined as the locomotion range of the platform. Actuator angular speed ω_{tip} is derived as shown in [8] and is given by

equations (11) and (12) for the cases of translational and rotational motion respectively.

$$\omega_{tip\min} = \left(\frac{(1+3a)^{-1} 2H(1+3a)g(3m+M)}{2mr((3\sqrt{3}h_o)^2 + (2H(1+3a))^2)^{1/2}} \right)^{1/2} \quad (11)$$

$$\omega_{tip} = \left(\frac{g(3+M/m)}{3r}\right)^{1/2} \quad (12)$$

From a design point of view, the objective is to choose platform parameter values such that the displacement per cycle is maximized. A set of design guidelines has been derived in [8] that leads first, to the selection of the coreless vibration micro-motor 4TH9-3006A manufactured by Jinlong Machinery & Electronics Co whose electromechanical parameters are listed on Table I and second, to a platform design whose basic design parameters are listed on Table II.

Table I
Vibrating motor SE-S4E specifications

Parameter	Value	Parameter	Value
Operating Voltage	0.9 *V*~1.6 *V*	Motor Weight	0.95 *g*
Starting Voltage	0.8 *V*	Motor diam.	4 *mm*
Starting Current	110 *mA*	Motor length	14.4 *mm*
Armature Resistance	10 Ω	Nominal speed	10000 *rpm*

Table II
Design parameters

Parameter	Value	Parameter	Value
r	0.00177 *m*	l	0.05 *m*
m	0.00021 *kg*	h_o	0.004 *m*
M	0.12 *kg*	μ	0.5

6 Closed orbit mode example

A number of simulation examples were presented in [8] that verify analytical results and demonstrate the platform motion capabilities. In this paper, a simulation example exemplifies the closed orbit operation and the platform deformation model. The platform parameters are those presented in Table II. According to Eq. (10), the upper bound of the closed orbit mode is $|\omega_c| = 9685.6 rpm$, while according to Eq. (8) the lower bound is $|\omega_{sl}| = 8519.4 rpm$. The motors speeds are set to $\omega_d = -9400 rpm$ and $\omega_f = 9400 rmp$, ω_e is zero. Fig. 6a depicts the accelerations of the platform. The spikes that are observed in the acceleration graph are due to switching from the deformable object model to the rigid body model. Fig. 6b presents the velocity of the platform and Fig. 6c its displacement. Clearly the platform operates in the closed orbit mode and exhibits zero net displacement.

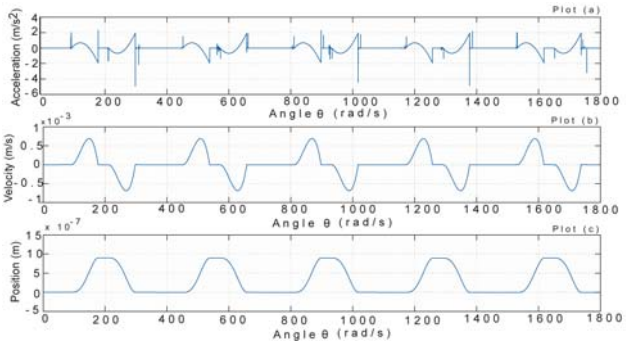

Fig. 6. Closed orbit simulation

Fig. 7 depicts the friction forces developed during the first cycle of operation. Initially, the platform is static, and the simulation uses the deformable object model. Friction is exerted only on legs A and C. Gradually the actuation forces and the friction forces on legs A and C increase. At some point friction forces reach the Coulomb level, then the platform starts to deform and forces are transmitted to leg C. When friction at all three legs has reached the Coulomb level, the platform accelerates, forward motion along the x-axis is induced, and simulation switches to the rigid body model. In a similar manner, dynamics alternate between deformable and rigid body models during the rest of the simulation.

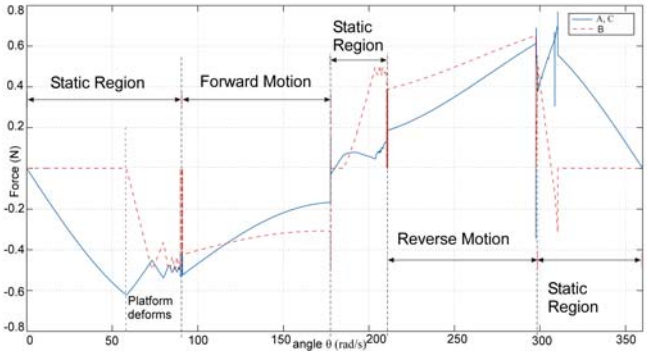

Fig. 7. Friction forces applied on legs A, B and C.

7 Closed loop speed control

Taking into account rotating mass accelerations, and neglecting the torque due to the rotating mass, Eqs. (3) become:

$$\begin{aligned} {}^b f_{ix} &= -(-mr\alpha\cos\theta + mr\omega^2\sin\theta)\sin\phi_i \\ {}^b f_{iy} &= (-mr\alpha\cos\theta + mr\omega^2\sin\theta)\cos\phi_i \\ {}^b f_{iz} &= -mg - mr\alpha\sin\theta - mr\omega^2\cos\theta \\ i &= \{d,e,f\}, \phi_i = \{60^o, 180^o, -60^o\} \end{aligned} \quad (13)$$

where $\alpha = \dot{\omega} = \ddot{\theta}$. The acceleration $\ddot{\theta}$ is generated by the micro-motor that is governed by Eq. (7). Initially the platform moves at a speed of 0.7mm/s. It is desired to decelerate the platform to 0.4mm/s. For the open loop control case, this is achieved by solving numerically the platform inverse dynamics, and then calculating the required actuators speeds. The reference velocities are $\omega_d = -1047 rad/s$ and $\omega_f = 1047 rad.s$ The solid line in Fig. 8 first plot, depicts the step response of the platform's

velocity. The platform displacement is defined as the position difference between two successive static phases (flat regions in Fig.2e and Fig.6c). Consequently, the platform velocity is measured once per actuation cycle, and the output is formed by applying a zero order hold operation. The peaks that appear in the platform velocity response are due to numerical errors and not due to fluctuations of the output. The solid line in Fig. 8, second plot, depicts the step response of the actuators angular velocity. It can be seen that during open loop operation, the transient period of the platform's response is approximately the same as that of the actuators velocity. This means that the platform almost rapidly acquires the velocity imposed by the actuators. Hence, it arises that an improvement of actuator's angular velocity response will result to an analogous improvement to the platform's velocity response.

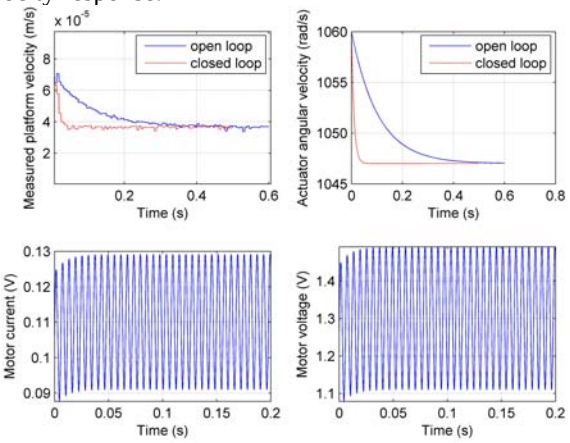

Fig 8. Transient response

To this aim, inverse dynamics plus a 2nd order stabilizing control law u given by eqs (14) are employed to first linearize eq (7) and then to control the response of the actuators. The controller is schematically presented in Fig. 9. A disturbance has been added in the inverse dynamics to model uncertainties.

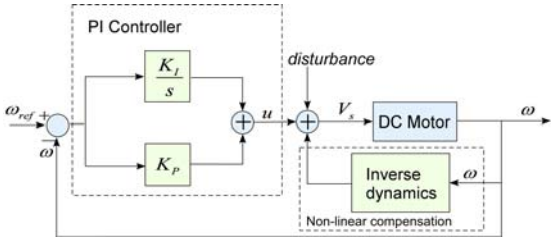

Fig. 9. Actuator closed-loop control

$$V_s = (k_t + \frac{Rb}{k_t})\omega + Rmgr\sin(\omega t)/k_t + \frac{cR}{k_t} + error + u_{control} \quad (14)$$

$$u_{control} = \omega_{ffwr} + K_P(\omega - \omega_{ref}) + K_I\int(\omega - \omega_{ref})dt$$

The controlled response of the platform and of the actuators is presented with dashed line in the first and second plots of Figs. 8 respectively. It is evident that the system time constant has reduced by a factor of ten. Figs. 8 third and fourth plot depict the voltages and currents of the actuators during the controlled response. Both values are within the permissible range of values specified by the micro-motor manufacturer in Table I.

8 Conclusions

The paper presented the analysis and design of a novel micro-robotic platform that is able to perform translational and rotational sliding with sub-micrometer positioning accuracy and develop velocities up to 1.5 *mm/s*. Dynamic models of the platform and of the actuators were provided. The modes of operation were defined. The transient response of the actuators was studied and their effect on the response of the platform was discussed. It is concluded that the platform translational response is analogous to that of the actuators. Hence by driving appropriately the actuators, the speed response of the platform can be controlled. The actuator speed control was achieved by employing model based controller and resulted in drastic improvement in speed control response.

9 Acknowledgements

The project is co-funded by the European Social Fund (75%) and National Resources (25%) – (EPEAEK II) - HRAKLEITOS

References:

[1] Jean-Marc Breguet, Reymond Clavel, Stick and Slip Actuators: design, control, performances and applications. *International Symposium on Micromechatronics and Human Science (MHS)*, (Nagoya), 1998, 89-95.

[2] Ferdinand Schmoeckel, Heinz Worn, Remotely controllable mobile micro-robots acting as nano positioners and intelligent tweezers in scanning electron microscopes (SEMs). *International Conference on Robotics and Automation*, Seoul, Korea May 21-26, 2001, 3903-3913.

[3] F. Schmoeckel, S. Fatikow, Smart Flexible Microrobots for Scanning Electron Microscope (SEM) Applications. *SPIE's 7th Int. Symp. On Smart Structures and Materials: Integrated systems*, Newport Beach, California, USA, 5-9 March 2000.

[4] J. Brufau, M. Puig-Vidal, et. al, MICRON: Small Autonomous Robot for Cell Manipulation Applications, *Proc. of the 2005 IEEE International Conference on Robotics & Automation*, Barcelona, Spain, April 18-22, 2005.

[5] Roland Büchi, Wolfgang Zesch, Alain Codourey, Inertial Drives for Micro- and Nanorobots: Analytical Study. *Proc. of SPIE Photonics East '95: Microrobotics and Micromachanical Systems Symposium*, Vol. 2593, Philadelphia, PA, Lynne E. Parker - Bellingham, WA, SPIE, 1995.

[6] Alain Codourey, Wolfgang Zesch, Roland Buchi, and Roland Siegwart, A Robot System for Automated Handling in Micro-World. *International Conference on Intelligent Robots and Systems*, Pittsburgh, PA, Aug. 1995, 3185-3191.

[7] Martel Sylvain et al., THREE-LEGGED WIRELESS MINIATURE ROBOTS FOR MASS-SCALE OPERATIONS AT THE SUB-ATOMIC SCALE. *Proc. of the 2001 IEEE International Conference on Robotics & Automation*, Seoul, Korea, May 21-26, 2001.

[8] P. Vartholomeos, E. Papadopoulos. Analysis and Design of a Novel Mini-platform Employing Vibration Micro-motors. *Proc. of the 2005 IEEE International Conference on Robotics & Automation*, Barcelona, Spain, April 18-22, 2005.

[9] E. Papadopoulos, I. Papadimitriou, Modelling, Design and Control of a Portable Washing Machine during the Spinning Cycle. *IEEE/ASMEInternational Conference on Advanced Intelligent Mechatronics System (AIM 2001)*, Como Italy, *8-11 July 2001*, 899-904.

[10] V.V. Badami, and N.W. Chibat, Home Appliances Get Smart, *IEEE Spectrum 35*(8), August 1998, 36-43

[11] E. Papadopoulos, , and G. Chasparis, Analysis and Model-Based Control of Servomechanisms with Friction, *ASME J. of Dynamic Systems, Measurement and Control*, *126*(4), December 2004.

[12] L.Sciavicco and B. Siciliano, *Modelling and Control of Robot Manipulators* (Springer-Verlag London Ltd, 2001).